Environmental x-ray considerations for bremsstrahlung-based surface potential determination

Kieran Wilson*and Hanspeter Schaub†
University of Colorado Boulder, Boulder, Colorado, 80309

A promising means to touchlessly determine the electrostatic potential of a target is to examine the bremsstrahlung x-ray spectrum emitted when energetic electrons impact it. Prior work has assumed these electrons to come from an electron beam mounted to a servicing craft, but it is shown here that ambient electrons in the local space environment could be used as well. X-rays induced by these electrons are examined as a noise source for the electron-beam based case, and the contribution of solar x-rays is also examined. While these additional sources of x-ray noise are found to not significantly impact previous analysis, new methods of utilizing ambient plasma-induced x-rays to estimate the potential on a target are evaluated. Additionally, a method of detecting debris objects within a few kilometers is suggested, utilizing the x-ray emissions induced by the environment.

Introduction

Objects in space charge through interactions with a variety of currents throughout their orbits. Photoelectric currents, driven predominantly by solar hard-UV light (also known as Vacuum Ultra Violet, or VUV), can result in positive potentials developing on a surface. This positive charging is balanced with plasma interactions, which can drive either positive or negative currents depending on the plasma properties. While some spacecraft carry instruments to sense their own electrostatic potential, sensing the potential on a nearby object without making contact is challenging. This paper extends prior work into a promising method for remotely sensing electrostatic potentials by combining an analysis of the x-ray environment at geostationary orbit–which can impact the promising method for remotely sensing electrostatic potentials in Reference [1]–with basic experimental results from a terrestrial test facility.

For spacecraft operating in the relatively cold, dense plasma present in Low Earth Orbit (LEO), the tendency is to charge a few volts positive in sunlight, and a few tens of volts negative in eclipse. While only mild potential levels are typically seen in LEO, previous research has suggested these levels can threaten spacewalking astronauts, and orbits passing through auroral zones can briefly experience potentials greater than -2 kV [2, 3]

However, in the sparser, hotter plasma environment found at geostationary orbit (GEO), objects can naturally charge to magnitudes of up to -30 kV during significant geomagnetic events [4]. This charging can cause significant problems relating to electrostatic discharges, including damaged solar arrays and potential loss of spacecraft [5–7]. In addition to single-craft charging, an increasing number of missions have been proposed which involve rendezvous between multiple bodies in regions of geospace prone to high levels of charging, such as servicing craft operating at GEO or NASA's planned Gateway in Lunar orbit. These spacecraft can potentially charge to different levels, particularly if one is eclipsing the other, or if they are composed of dissimilar materials or surface coatings [7, 8]. While many operational concepts include mechanisms to equilibriate two craft to the same potential prior to docking to minimize arcing risk, there can still be significant (milli-Newton level) forces acting between the two craft due to electrostatic interactions. These forces can be significant perturbations during rendezvous, and may need to be taken into account by the GNC system.

In addition to well known effects of spacecraft charging, concepts have been recently developed to harness electrostatic forces and torques between spacecraft for touchless detumbling or re-orbiting uncooperative targets. The electrostatic tractor concept uses an electron gun to charge the space tug positively and the space debris negatively, creating a positive electrostatic force [9, 10]. Many of these concepts require knowledge of the target's charge for feedback control, and the ability to measure the charge on a space object remotely would also benefit servicing or rendezvous scenarios which may otherwise risk dangerous arcing hazards. This concept is shown in Figure 1. For uncooperative charging scenarios it is often only possible to obtain charge data from the active craft. The ability to measure spacecraft potentials touchlessly could also contribute to the overall understanding of spacecraft charging

*Graduate student, Ann and H.J. Smead Aerospace Engineering Department
†AIAA and AAS Fellow, Glenn L. Murphy Endowed Chair, Ann and H.J. Smead Aerospace Engineering Department

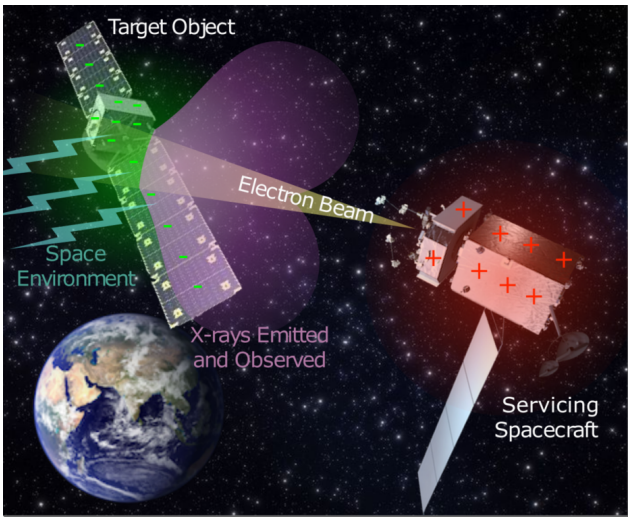

Fig. 1 Concept of the operating electrostatic tractor, utilizing an electron beam to control the charge on a debris body.

through changing environments. However, currently it is only possible to measure the potential on an instrumented craft itself, without determining any charging properties of an uninstrumented object.

Reference [11] presents a method for remotely measuring the electrostatic potential on an object in space. When energetic electrons impact a surface, they release a continuum of x-rays known as bremsstrahlung. The resultant x-ray spectrum can be deconvolved to determine the landing energy of the electrons impacting the surface, with the additional benefit of generating characteristic peaks in the radiation that can be used to determine the target's elemental composition. An example of the spectra generated by 5.5 and 6.5 keV electron beams on aluminum targets are seen in Figure 2, with different landing energies noticeable from the different upper limits of the spectra. Assuming knowledge of the electrons at a co-orbiting observer craft, either from measurement of the local plasma or by setting the energy of an electron gun illuminating the target, the relative potential between the observer and the target can be inferred.

For a monoenergetic electron beam, the landing energy can be determined by examining the highest energy photons observed. Per the Duane-Hunt law, the energy of the x-rays emitted by the electrons cannot exceed the landing energy of the electrons, so the upper energy limit of the x-ray spectrum is the highest energy observed [12]. However, this method is not particularly robust, as the case where an electron is fully stopped and converts its entire landing energy to a single photon is exceedingly rare, providing few references to estimate the landing energy. A more robust method for determining the landing energy of a monoenergetic electron beam is put forward by Reference [13], where a line is fit to the upper energy portion of the spectrum. The interception of this line of fit with the x-axis represents the landing energy. This method was used by Reference [14] to determine that the landing energy of the electron beam in the ECLIPS chamber can reliably be determined to within a few percent.

The Autonomous Vehicle Systems (AVS) Lab's Experimental Charging Laboratory for Interaction of Plasma and Spacecraft (ECLIPS) is used for all experiments. The x-ray detector is mounted on a rotational stage at the edge of the chamber (diameter approximately 50 cm), while the target is located in the middle of the chamber. Bremsstrahlung radiation is strongly directionally dependent, so the ability to sweep through angles is crucial to fully characterizing this method for remote potential sensing. The target plate potential can be controlled independently of the electron beam, so the landing energy determination enables the plate potential to be determined if the beam energy is known.

Experimental tests were conducted in a space environment simulation chamber, using an electron gun capable of energies up to 30 keV. An Amptek X123 Si-PIN diode x-ray spectrometer was used to measure the x-ray spectrum resulting when the electron beam irradiated a target. This detector has a 1 mil (0.0254 mm) thick frontal beryllium window, and has an effective range from 1 to 30 keV, making it well suited to the energies of interest here [15]. Additionally, this instrument has flight heritage aboard the MinXSS-1 solar spectrometer mission.

An aluminum plate was used as a target, and the x-ray detector held approximately 20 cm from the target, with an angle of 70° from the beam. The beam energy was varied from 5.5 to 6.5 keV, and currents from 0.5 to 1.5 μA. These tests, shown in Figure 2, have indicated that it is indeed possible to determine the landing energy of the electron beam

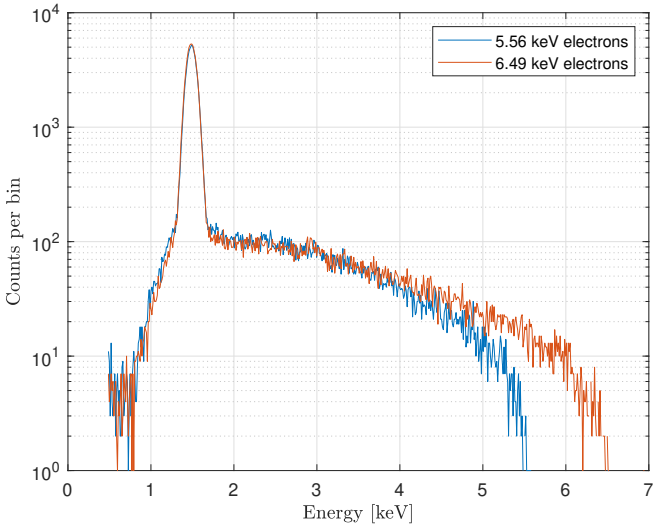

Fig. 2 X-ray spectra generated from two different electron energy levels impacting an aluminum target, beam current of 10 μA. The target potential in both cases was 0V, so the landing energy was dictated only by the beam energy.

on a surface in a space-like environment, with landing energy determinations within 100 eV of the experiment settings. Furthermore, the peak in photon counts seen at 1.56 keV corresponds to the characteristic peak for aluminum, providing a confirmation of material identification.

Reference [14] experimentally demonstrates the fundamentals of this method for remotely determining the potential and material composition of a surface, though only using a limited range of target potentials and beam energies. One significant result was demonstrating that the landing energy of the electrons could be determined to within a few percent error, while also determining the elements in a material from their constituent characteristic peaks. These prior tests covered two materials, 6061 aluminum and Inconel, and used only flat target plates that were rotated with respect to the detector, or held at a constant angle while the detector was swept around the target.

While previous work has demonstrated the theoretical [1] and experimental [14] viability of the concept, these have been done for the case of an electron beam in a pure vacuum, and neglected environmental considerations. This work extends the prior analysis to look at the impact of GEO electron fluxes, which can generate additional bremsstrahlung radiation, and solar x-ray contributions. Additionally, passive sensing for determining electrostatic potential of a target (which relies on the ambient plasma to generate x-ray fluxes without requiring an electron beam) and applications of ambient plasma-induced x-rays are discussed.

Prior observations of environmentally induced x-rays

Bremsstrahlung due to energetic local electrons are a frequent observation for orbital x-ray detectors. These observations typically take one of three forms: energetic particles precipitating into the atmosphere and emitting bremsstrahlung radiation, bremsstrahlung occurring on the spacecraft in view of the sensor, or occurring within the sensor itself. The BATSE instrument counted numerous examples of x-ray bursts which were traced to electron bremsstrahlung on the spacecraft or in the instrument [16]. Instrument design, such as that for the WFIRST telescope, now frequently includes an evaluation of electron induced bremsstrahlung when assessing instrument performance in regions with known populations of energetic electrons [17, 18]. Reference [19] presents a general overview of observations of bremsstrahlung generated by energetic electrons precipitating into the atmosphere, while Reference [20] examines these bremsstrahlung spectra to determine the energy distribution of the source electron population. Bremsstrahlung from energetic plasma electrons has also been observed on the lunar surface [21].

Additionally, Reference [22] presents a method to remotely determine the occurrence of charging events using environmental electron fluxes. They examined the increase in high energy bremsstrahlung that would be expected to accompany hot electrons in geomagnetic storm conditions at GEO, and found that it may be possible for a co-orbiting

spacecraft to observe these x-rays as signatures of charging events. However, the method presented here only indicates a proxy of conditions which are conducive to spacecraft charging, but does not enable an evaluation of the extent of charging.

Ambient plasma-induced x-rays

Bremsstrahlung radiation with energies that can be captured by an x-ray detector can be generated by any electrons with energies above ≈1 keV. However, the high resolution energy dispersive detectors considered for remote potential sensing applications here work only in finite energy regions. For the Si-PIN diode in the Amptek X123, the detection efficiency begins to fall off above 12 keV, and limits the detection energy to approximately 1-30 keV [15].

Bremsstrahlung radiation is generated up to the energy of the incident electron, so even a 1 MeV electron would be expected to have some contribution in the 1-30 keV range. However, the flux of electrons with a given energy decreases rapidly as energies increase, so the contributions of higher energy electrons can be neglected. Geospace plasma, particularly in the geostationary orbit region, is dominated by electrons and protons, and both are capable of generating bremsstrahlung radiation. However, the much higher mass of protons means they require orders of magnitude more kinetic energy than electrons to achieve significant bremsstrahlung yields, so their contributions to the x-ray spectrum are neglected. Additionally, the electron flux at GEO is assumed to be isotropic. Even though bremsstrahlung has strong directional components depending on the angle of the incident electron, prior work on plasma-generated bremsstrahlung indicates the resultant thick target spectrum can be assumed to be isotropic [23].

The bremsstrahlung yield is dependent on the energy of the incident electron, and on the atomic number of the target material. Spacecraft generally make extensive use of aluminum alloys in their construction, and aluminized coatings are a major component of the multi-layer insulation typically used to insulate spacecraft.

According to the NIST ESTAR database of electron stopping powers in various materials, a 20 keV electron will be stopped in 7.5 μm of aluminum [24]. Assuming an incident electron flux that is isotropically distributed across 2π steradians, the mean stopping distance should fall within 4.5 μm of the material surface. The random walk nature of successive electron-atom interactions also serves to reduce this distance, such that electrons can be expected to deposit their energy very close to the surface. Therefore, the assumption that only coatings and surface materials is valid for this approximation.

An aluminum coated spacecraft is assumed for this work. In practice, a spacecraft would likely have surfaces coated in thermal control paint such as AZ-93, and solar arrays covered in glass and likely coated with a conductive film such as indium tin oxide. While the elemental composition of AZ-93 is not available in the literature, it is known to use a silicate-based binder [25]. Silicon has atomic number 14, while aluminum is 13, so the silicate binder will have similar bremsstrahlung and characteristic radiation efficiencies to aluminum. The specification provides for application of AZ-93 to a depth of 5 mils, or 0.127 mm, which is far larger than the maximum range of electrons in the material [25].

Two components of the x-ray spectrum require separate calculation to simulate the complete electron-induced x-ray spectrum: the discrete energy emission of characteristic radiation, and the bremsstrahlung continuum spectrum.

Characteristic radiation occurs when an incident electron removes an inner shell electron from an atom, at which point an outer shell electron relaxes to fill the vacancy. The energy difference between the two orbitals is released as an x-ray. The energy difference between two orbitals is unique to each element, and as such the emitted photons are characteristic to a specific element and can be used for elemental identification. The characteristic radiation yield, defined as the number of photons of characteristic radiation (from the dominant K_α transitions) generated per incident electron of a specific incident energy can be estimated as

$$I_p = N\left(\frac{E_e}{E_k} - 1\right)^{\alpha} \tag{1}$$

where, for aluminum, $N = 1.4\times10^{-5}$, $\alpha = 1.63$ and the energy of characteristic emission $E_k = 1.49$, while E_e represents the incident electron energy. Electrons with energy less than E_k are not capable of generating characteristic emission in this transition, so I_p for these cases is zero. For a given number of incident electrons N_e of a specific energy E_e, the expected number of characteristic photons can be computed.

However, the detector will not observe an infinitely narrow representation of the characteristic radiation with a single specific energy. Instead, the detector observes a Gaussian distribution with a width given by the full width at half maximum (FWHM). For the detector used in the experimental work here, the FWHM was found to be approximately

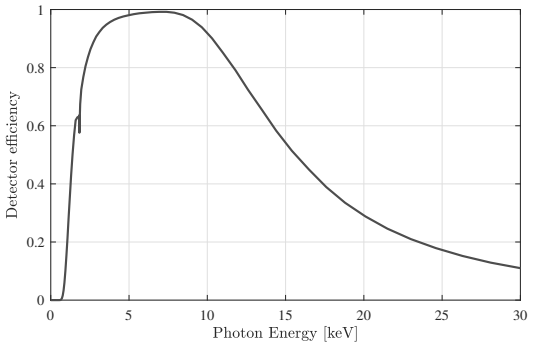

Fig. 3 Efficiency (in photons detected per incident photon) for the Amptek X123 500μm thick Si-PIN diode detector with 1 mil thick frontal Be window.

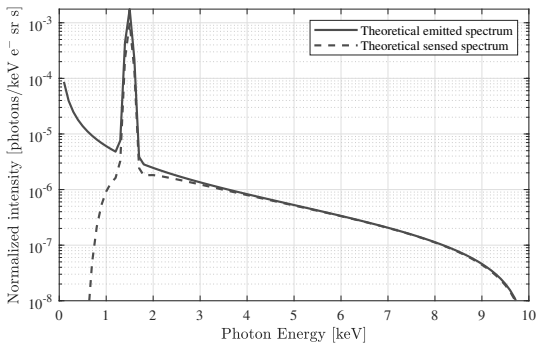

Fig. 4 Analytical x-ray spectrum for 10 keV electrons with and without accounting for detector efficiency.

140 eV. FWHM can be converted to standard deviation σ by the relation

$$\sigma = \frac{2\sqrt{2\ln 2}}{FWHM}. \tag{2}$$

The distribution sensed by the detector should contain $I_p \cdot N_e$ photons, but redistributed into a Gaussian function with the given standard deviation. This is achieved by using the analytic integral of the Gaussian function. As the integral is known to be $I_p \cdot N_e$, and σ is defined by the sensor, the height of the sensed peak can be determined, and the characteristic spectrum is fully defined.

A variety of models are available to simulate the bremsstrahlung spectrum from monoenergetic electrons on thick targets, many of which are provided in review by Reference [26]. The electron is assumed to be fully stopped in the target, so a thick target model is used. These models can be divided into two main categories: analytic expressions, often empirically derived from sample data sets, and Monte Carlo-based simulations. While the Monte Carlo simulations can be more accurate than the analytic expressions, they have the disadvantage of requiring significantly more computational resources; the analytic expressions are generally accurate to within 20%, which is not much worse than Monte Carlo simulations, and adequate for the analysis performed here [26]. The equation selected for use here is an empirical fit valid for photons in the 0.5-20 keV range and elements from $Z = 4$ to $Z = 83$, while covering electron energies up to 38 keV. While electron energies considered in this work exceed this value and are subject to reduced accuracy, the results are still considered sufficient for the accuracy desired here [27].

$$\Delta I = C\sqrt{Z}\frac{E_o - E}{E}\left(-73.90 - 1.2446E + 36.502\ln Z + \frac{148.5E_o^{0.1293}}{Z}\right) \times \left[1 + (-0.006624 + 0.0002906E_o)\frac{Z}{E}\right]\Delta E \tag{3}$$

A final complication is introduced with real sensors. The detector consists of a frontal window, designed to filter out low energy photons (such as those in the visible or UV portions of the spectrum) to avoid detector saturation, followed by a Si-PIN diode. When photons penetrate the window, which is 1 mil (0.025 mm) thick Beryllium, they interact with the diode. As the photon deposits energy into the diode, it results in the formation of electron-hole pairs. The electrons are then drawn toward an electrode by an electric field, where they are then counted and the energy of the incident photon inferred by the number of electron-hole pairs generated [15].

However, it is possible for high energy photons to pass through the detector without depositing a significant fraction of their energy. Therefore, both low energies and high energies are attenuated by the detector, and only a range of energies in the middle are accurately measured. Figure 3 illustrates the energy-dependent efficiency for the specific detector used here, while Figure 4 illustrates the impact of accounting for the detector efficiency on the sensed spectrum.

This theoretical model is compared to the experimental results obtained, and the resultant curves are shown in Figure 5. Although Equation 3 is typically considered to be accurate to within 20%, the strong qualitative agreement between the theoretical and experimental spectra suggests that this equation is a good approximation for the energies and elements under consideration here.

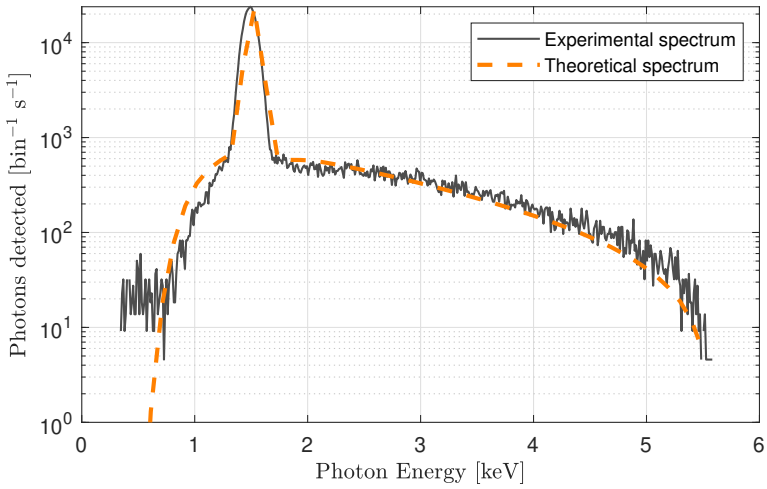

Fig. 5 Comparison of theoretical spectrum from Equation 3 and experimental results. Beam parameters: 10μA, 5.5 keV.

A year-averaged GEO flux was obtained from SPENVIS, using the IGE-2006 model for trapped electron fluxes [28]. This model provides 3 flux outputs: a mean, a lower bound and an upper, as seen in Figure 6. The electron energies are sorted into logarithmically spaced bins, and the 16 bins from 0.92 keV to 130 keV are used here. Though the model includes electron fluxes for energies up to 5 MeV, the diminishing numbers of electrons at increasing energies means the contribution of those electrons to the 0-30 keV x-ray spectrum is limited.

From this set of electron energy distributions, combined with Equations 1 and 3, the emitted x-ray spectrum can now be approximated. This is done iteratively, with the assumption of all electrons in a given bin having the initial energy of that bin (ie, all electrons in the 0.92-1.2 keV bin are assumed to have an energy of 0.92 keV). Figure 7 illustrates the x-ray spectrum contributions of each energy bin, and the total x-ray flux that would be generated for the IGE-2006 mean electron flux case.

In relative terms, the lower electron flux case from the IGE-2006 model resulted in 31% fewer x-ray photons being generated relative to the mean case. The upper electron flux case resulted in a 46% increase in photon emission relative to the mean.

The goal of this work is ultimately to determine the electrostatic potential on a co-orbiting object touchlessly. The bremsstrahlung spectrum from ambient electrons provides an intriguing option for doing so without requiring an active electron beam to excite bremsstrahlung x-rays.

Spacecraft tend to charge negatively in GEO, and the scenario where an electron beam is used to generate bremsstrahlung radiation on a target object will also results in negative charge accumulating on the target. As it charges negatively, it will effectively shift the energy of incident electrons. A spacecraft charged to -10kV, for example, will repel any incident electrons with less than 10 kV. Therefore, the electron spectrum will be shifted by 10 kV, as seen in Figure 8, which results in the change in x-ray photon spectrum seen in 9.

The change in emitted x-ray quantities provides a means of determining the charge state of an object without requiring spectrum-based analysis. If the servicing craft can measure the local electron population, then the potential of the target can be inferred by examining the reduction in x-ray emission in the 0-30 keV range. While this would be more challenging to implement if the local plasma conditions were varying with time as the anticipated bremsstrahlung spectrum would have to be accurately recomputed for each new set of plasma conditions, it could be useful in indicating changing surface potentials in cases where the plasma remains relatively constant. Such circumstances are found naturally when a spacecraft crosses from sunlight to eclipse conditions (or in a rendezvous scenario, when the servicer eclipses the sunlight on the target).

During rendezvous of the Orion crew module with NASA's planned Lunar Gateway, the Orion capsule will be in the shadow of the Gateway during the terminal rendezvous phase. Analyses have shown that the change in photoelectric current could result in potential differences of several kV between the two bodies, posing electrostatic discharge risks at contact [8]. The ability to measure the relative potentials between the objects, or the change in potential of the Orion

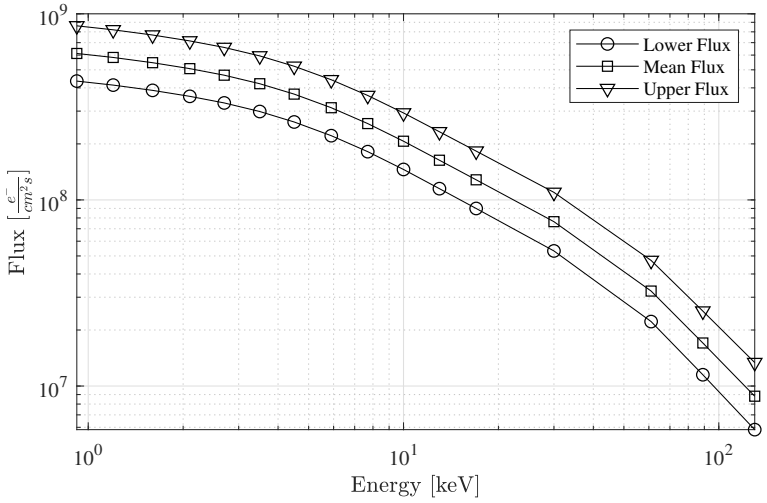

Fig. 6 The electron flux at GEO for IGE-2006 model lower, mean and upper fluxes. Points from the model are illustrated by the markers, the lines are for illustrative purposes only.

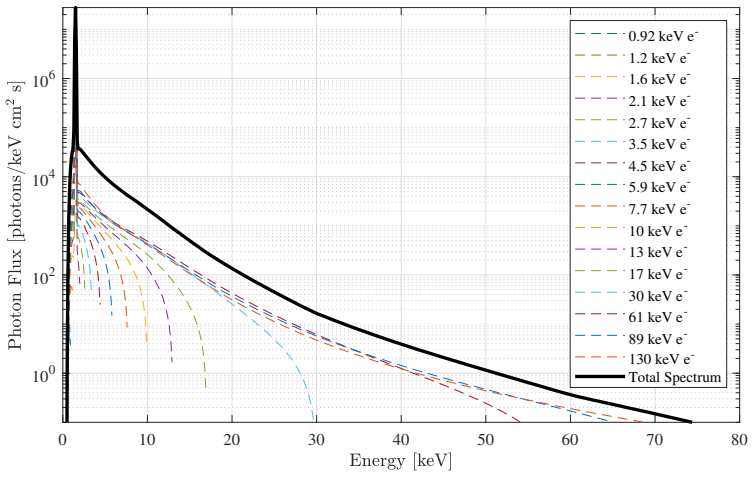

Fig. 7 X-ray spectrum due to mean electron flux conditions at GEO.

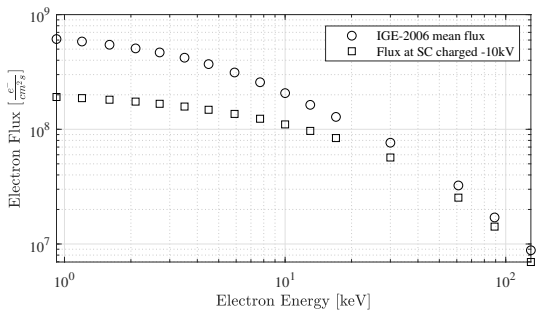

Fig. 8 Electron flux from the IGE-2006 mean flux and that observed by a spacecraft charged to -10 kV.

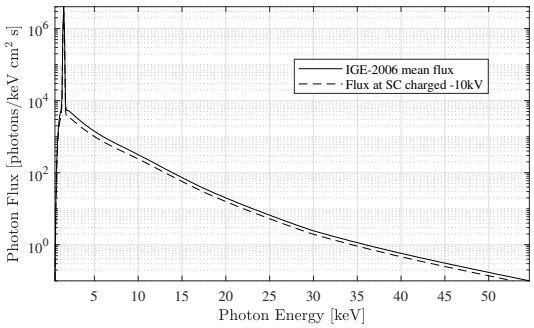

Fig. 9 X-ray photon flux from the IGE-2006 mean flux and that observed by a spacecraft charged to -10 kV.

module as it moves into eclipse, could help indicate the presence of hazardous potential differences.

It is worth noting that the simulations here, that the x-ray flux decreases as a spacecraft charges, runs somewhat counter to the conclusions of Reference [22] in their analysis of using x-ray fluxes as proxy indicators of charging events. However, these two analyses rely on fundamentally different assumptions: here it is assumed that the plasma conditions are near steady state, while the work of Reference [22] assumed the spacecraft were charging due to changing plasma conditions. The authors therefore examined high energy bremsstrahlung emitted by the high energy electrons (40 to 180 keV) associated with geomagnetic storm conditions, and did not look a the contributions of more numerous but lower energy electron populations that are significant even in quiet conditions.

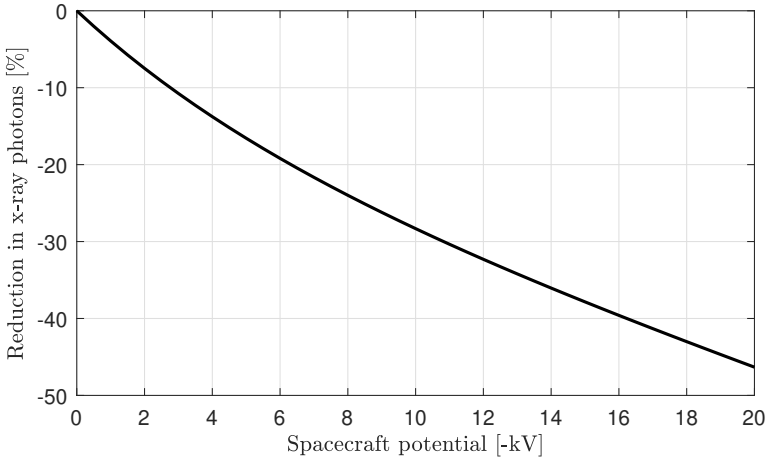

Fig. 10 Change in total x-ray photon emission due to plasma electron bremsstrahlung as a function of spacecraft potential.

Solar x-ray contribution

The sun is a significant source of x-rays in space, which could conceivably interfere with efforts to use x-ray spectra to measure the landing energy of electrons. A number of missions have flown x-ray spectrometers in Earth orbit to observe the sun, and these spectra could be used to determine the contribution of the solar x-ray spectrum to a spectrum that would be sensed in a potential measurement scenario. Two missions, the MinXSS-1 and MinXSS-2 cubesat solar observatories, flew variants of the x-ray detector used in the experimental part of this work [29].

MinXSS-1 operated in 2016, and two sample spectra from this mission, preprocessed to Level 1 and obtained from [30], are shown in Figure 11.

It is assumed that the sensor is oriented such that the sun line of sight is excluded from the sensor's field of view, but

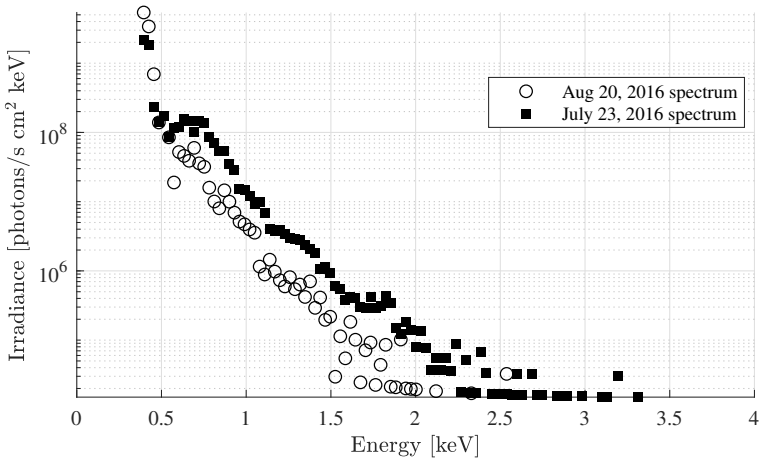

Fig. 11 The solar x-ray spectrum observed by MinXSS-1. July 23 was the date of 2016's most significant flare event, an M7.6, and illustrates enhanced x-ray flux relative to the quiet August 20th spectrum [30].

the sun is illuminating the object of interest. X-rays incident on a surface typically do not reflect, but can excite the release of characteristic x-rays from the surface material, a process known as secondary fluorescence. Any incident x-ray with an energy above the characteristic energy of the atom it is interacting with can result in secondary fluorescence. An equation for fluorescence yield was developed by Reference [31], and represents the number of characteristic photon emissions per incident photon:

$$\omega_K = \frac{10^{-6}Z^4}{1 + 10^{-6}Z^4} \tag{4}$$

For aluminum, this yields an efficiency of approximately 0.03, which matches well with the experimental data compiled by [32].

Solar-induced secondary fluorescence has been used on a variety of spacecraft missions to determine the elemental composition of celestial bodies, including the Moon and asteroids [33].

Therefore, for each photon with an energy over 1.49 keV, 0.03 characteristic x-rays can be expected to be emitted from the target. Characteristic radiation emission is isotropic, so only half of these x-rays will escape from a flat surface. For a spacecraft made of aluminum with an area of 5 m^2, integrating the MinXSS-1 data for the nominal August 20th spectrum and then multiplying by ω_k, this yields 2.5×10^7 photons emitted per second with an energy of 1.49 keV. The same analysis performed on the July 23, 2016 flare data yields an x-ray flux nearly 6 times larger, at 1.4×10^8 photons per second.

Ultimately, the solar x-ray contribution to the sensed x-ray spectrum from the target will be fairly negligible, only serving to increase the flux of characteristic x-rays. Incident photons with energies above the characteristic energy of the surface elements will be absorbed by the material but can contribute to characteristic emission, while those with energies below E_k will primarily be absorbed without inducing secondary fluorescence. For the nominal solar spectrum, it is expected that only a few tens of additional photons will be observed per second by a 75 mm^2 detector at a distance of 10 meters.

While the servicing spacecraft can be oriented to avoid having solar photons directly incident on the sensor aperture, the cosmic x-ray background is much harder to exclude. However, the flux levels are quite low, with estimates on the order of 10 photons cm^{-2} s^{-1} sr^{-1} keV^{-1} in the keV range. For a 75 mm^2 detector with a 10° field of view, this yields a flux of around 1 photon per minute, a level that will likely not have any significant impact on this technique.

Spectrum with environmental noise contributions

Ultimately, the bremsstrahlung-based method for determining the potential of a target is likely to be used in active charge control scenarios, such as the Electrostatic Tractor [9]. A nominal electron beam current for such a scenario may be on the order of 10 μA. Figure 12 illustrates the relative magnitudes of the bremsstrahlung radiation from the electron beam and the ambient plasma, assumed to be the IGE-2006 mean flux. The solar x-ray spectrum adds only to

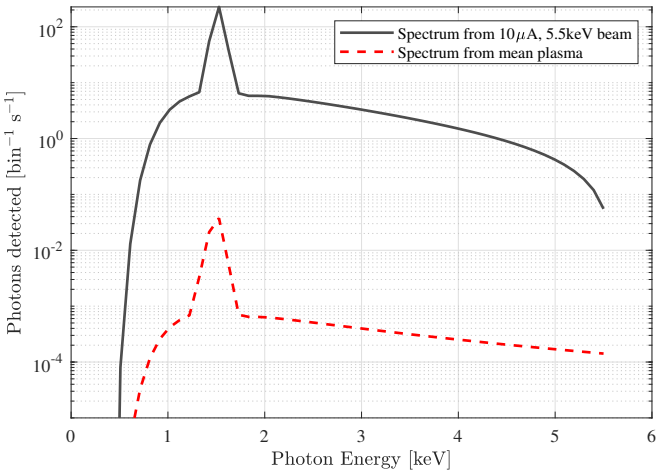

Fig. 12 Simulation of sensed x-ray spectrum for a 10 μA electron beam and ambient plasma electron fluxes, using the IGE-2006 mean flux. The target is assumed to be an isotropically emitting point source equivalent to a 5 m^2 aluminum spacecraft.

the characteristic radiation, and has no contribution to the bremsstrahlung continuum, so is not shown here. However, the hot plasma electron flux does contribute to the bremsstrahlung spectrum, but at a level that is approximately 4 orders of magnitude smaller than the beam-induced flux. This makes sense, as the electron beam current in this scenario is 10 μA, while the cumulative plasma current (neglecting charging effects) is approximately 0.7 nA, roughly 3.5 orders of magnitude smaller. Higher energy electrons in the plasma will contribute greater numbers of photons than lower energy electrons.

Both spectra are treated as isotropic point sources 10 meters from a detector with a 75 mm^2 sensor. In reality, the electron beam contribution is likely to behave in a point-source like manner, but the x-ray emission from it is not isotropic. Instead the sensed flux will depend significantly on the angle between the incident electron beam and the detector; though prior experimental work by the authors has indicated that even for small separation angles (for the case where the detector is positioned near the electron beam) significant fluxes can still be observed. The plasma-induced x-rays will also be isotropic, but are less accurately modeled by the point source approximation. However, accurately modeling this distribution requires knowledge of the target geometry and relative attitude, which is beyond the scope of this work.

The local plasma is fairly insignificant contribution to the sensed spectrum, and will not significantly impact the ability to determine the landing energy of the electrons (and therefore the relative potential). Likewise, the solar x-ray contribution to only the characteristic radiation will not impact the determination of electron beam landing energy.

Debris sensing SSA applications

The dominant means of tracking objects in space currently are by use of radar arrays, or optical tracking, which relies on sunlight reflected by target objects. Both of these methods are typically ground-based, have limited resolution and sensitivity at GEO, and pose challenges in integrating into a spacecraft [34]. The mechanisms described here which lead to x-ray emission from a body apply to any solid in space. Therefore an object, such as difficult-to-track debris objects, in a region with either solar x-rays or energetic electron populations will emit x-rays. These x-ray emissions could have implications for space situational awareness (SSA) applications, providing a means of detecting co-orbiting debris objects passively. This can be particularly useful in a GEO context, where many large objects orbit with very low relative velocities but can be closely spaced. Ground-based observations of spacecraft in GEO are limited to tracking objects greater than around 1 meter in size, and have limited positional resolutions [35]. Therefore, it would be advantageous to be able to passively sense other debris objects passing in a spacecraft's vicinity to improve the debris catalogue and potentially inform avoidance maneuvers to mitigate collision risks.

Combining the results of the IGE-2006 mean electron spectrum and the mean solar induced fluorescence, approximately 2.8×10^{10} x-ray photons will be emitted per second from a 5 m^2 aluminum debris object, such as a

defunct spacecraft. In practice elements heavier than aluminum, such as indium-tin compounds used to coat solar panels, or nickel alloys used in rocket motor nozzles, will have reduced characteristic radiation yields (due to the increase in characteristic energy) but increased bremsstrahlung yields. However, the aluminum approximation can be used to determine the feasibility of detecting these emissions from a co-orbiting spacecraft.

A few assumptions about the sensor and detection thresholds are made. First, the sensor is assumed to require detection of 10 photons over a 20 second integration period to provide a reasonable reliability. As earlier, the photons are assumed to be emitted from the object are isotropically, and a sensor like the Amptek SDD with a with a mean efficiency in the energy region of interest of 90% and a detector area of 75 mm^2 is used. For this case, a separation of some 780 meters or less yields the signal required to identify the presence of a nearby object; this rises to nearly 1 km for the IGE-2006 upper electron flux case. The detector sensitivity could be increased by the use of x-ray optics, like those that were developed for the NICER x-ray observatory mission which have an effective collection area of 44 cm^2 at 1.5 keV [36]. Adding these optics extends the detection range to nearly 6 km (over 7.2 km in the upper electron flux case). Other options, from larger or more efficient optics, or increased integration times, could improve the sensitivity of this method.

Conclusions

Although environmental contributions to the sensed x-ray spectra are found to not have a significant impact on the ability to determine the relative potential between a servicer and a target, they are able to provide an alternative, passive form of electrostatic potential estimation. The introduction of environmentally-induced x-ray fluxes also allows for the use of x-rays in space situational awareness applications, where spacecraft could determine the presence of nearby debris objects by their x-ray emissions.

Future work will examine more realistic distributions of materials and non-planar surfaces. Both of these factors complicate the analysis, but will yield high fidelity models of the x-ray spectra generated by the interaction of the object with the space environment. As noted previously, higher atomic number materials will experience reduced characteristic radiation yields, but increased bremsstrahlung yields. Finally, the isotropic x-ray emission assumption should be rigorously analyzed. Although the electron flux may be isotropic, the direction of bremsstrahlung emission known to be strongly dependent on the incident electron energy, so while the isotropic emission assumption may be adequate for relatively low (keV) energies, once electron energies reach 10s or 100s of keV this assumption may no longer be valid.

References

[1] Wilson, K., and Schaub, H., "X-Ray Spectroscopy for Electrostatic Potential and Material Determination of Space Objects," *IEEE Transactions on Plasma Science*, 2019.

[2] M. R. Carruth, R. S. M. M., D. Ferguson, "ISS and Space Environment Interactions Without Operating Plasma Contactor," Tech. rep., NASA, 2001.

[3] Anderson, P. C., "Characteristics of spacecraft charging in low Earth orbit," *J. Geophys. Res.*, Vol. 117, No. A7, 2012, p. A07308. doi:10.1029/2011JA016875, URL `http://dx.doi.org/10.1029/2011JA016875`.

[4] Mullen, E. G., Gussenhoven, M. S., Hardy, D. A., Aggson, T. A., and Ledley, B. G., "SCATHA Survey of High-Voltage Spacecraft Charging in Sunlight," *Journal of Geophysical Research*, Vol. 91, No. A2, 1986, pp. 1474–1490. doi:10.1029/JA091iA02p01474.

[5] Katz, I., Davis, V. A., and Snyder, D. B., "Mechanism for Spacecraft Charging Initiated Destruction of Solar Arrays in GEO," *36^{th} Aerospace Sciences Meeting and Exhibit*, Reno, NV, 1998.

[6] Ferguson, D. C., Hoffmann, R. C., Engelhart, D. P., and Plis, E. A., "Voltage Threshold and Power Degradation Rate for GPS Solar Array Arcing," *IEEE Transactions on Plasma Science*, Vol. 45, No. 8, 2017, pp. 1972–1975. doi:10.1109/TPS.2017.2694387.

[7] Lai, S. T., *Fundamentals of Spacecraft Charging: Spacecraft Interactions with Space Plasmas*, Princeton University Press, 2011.

[8] Goodman, M., Paez, A., Willis, E., and DeStefano, A., "An Analytic Model for Estimating the First Contact Resistance Needed to Avoid Damaging ESD During Spacecraft Docking in GEO," *Applied Space Environments Conference*, 2019.

[9] Schaub, H., and Moorer, D. F., "Geosynchronous Large Debris Reorbiter: Challenges and Prospects," *The Journal of the Astronautical Sciences*, Vol. 59, No. 1–2, 2014, pp. 161–176.

[10] Bengtson, M., Wilson, K., Hughes, J., and Schaub, H., "Survey of the electrostatic tractor research for reorbiting passive GEO space objects," *Astrodynamics*, Vol. 2, No. 4, 2018, pp. 291–305.

[11] Wilson, K., and Schaub, H., "Prospects and Challenges of Bremsstrahlung-based Electrostatic Potential and Material Composition Determination for Spacecraft," Proceedings of the 15th Spacecraft Charging Technology Conference, 2018.

[12] Duane, W., and Hunt, F., "On X-Ray Wave-Lengths," *Phys. Rev.*, Vol. 6, 1915, pp. 166–172. doi:10.1103/PhysRev.6.166.

[13] M. Lamoureux, P. C., "General deconvolution of thin-target and thick-target Bremsstrahlung spectra to determine electron energy distributions," *Radiation Physics and Chemistry*, Vol. 75, No. 10, 2006.

[14] Wilson, K., and Schaub, H., "Electron-Induced X-Rays for Remote Potential Sensing," *Applied Space Environments Conference*, 2019.

[15] "XR-100CR Si-PIN x-ray detector," Tech. rep., Amptek, Inc., 2018.

[16] Horack, J. M., Fishman, G. J., Meegan, C. A., Wilson, R. B., and Paciesas, W. S., "BATSE observations of bremsstrahlung from electron precipitation events," *AIP Conference Proceedings*, Vol. 265, No. 1, 1991, pp. 373–377. doi:10.1063/1.42765.

[17] Tuszewski, M., Cayton, T. E., Ingraham, J. C., and Kippen, R. M., "Bremsstrahlung effects in energetic particle detectors," *Space Weather*, Vol. 2, No. 10, 2004. doi:10.1029/2003SW000057, URL https://agupubs.onlinelibrary.wiley.com/doi/abs/10.1029/2003SW000057.

[18] Kruk, J. W., Xapsos, M. A., Armani, N., Stauffer, C., and Hirata, C. M., "Radiation-induced Backgrounds in Astronomical Instruments: Considerations for Geosynchronous Orbit and Implications for the Design of theWFIRSTWide-field Instrument," *Publications of the Astronomical Society of the Pacific*, Vol. 128, No. 961, 2016, p. 035005. doi:10.1088/1538-3873/128/961/035005.

[19] Imhof, W. L., "Review of energetic (> 20 ke V) bremsstrahlung X-ray measurements from satellites," *Space Science Reviews*, Vol. 29, No. 2, 1981, pp. 201–217. doi:10.1007/BF00222145, URL https://doi.org/10.1007/BF00222145.

[20] Xu, W., and Marshall, R. A., "Characteristics of Energetic Electron Precipitation Estimated from Simulated Bremsstrahlung X-ray Distributions," *Journal of Geophysical Research: Space Physics*, Vol. 124, No. 4, 2019, pp. 2831–2843. doi:10.1029/2018JA026273.

[21] Kamata, Y., Takeshima, T., Okada, T., and Terada, K., "Detection of X-ray fluorescence line feature from the lunar surface," *Advances in Space Research*, Vol. 23, No. 11, 1999, pp. 1829 – 1832. doi:https://doi.org/10.1016/S0273-1177(99)00539-6, URL http://www.sciencedirect.com/science/article/pii/S0273117799005396, the Moon and Mars.

[22] Ferguson, D. C., Murray-Krezan, J., Barton, D. A., Dennison, J. R., and Gregory, S. A., "Feasibility of Detecting Spacecraft Charging and Arcing by Remote Sensing," *Journal of Spacecraft and Rockets*, Vol. 51, No. 6, 2014.

[23] McCall, G. H., "Calculation of X-ray bremsstrahlung and characteristic line emission produced by a Maxwellian electron distribution," *Journal of Physics D: Applied Physics*, Vol. 15, No. 5, 1982, pp. 823–831. doi:10.1088/0022-3727/15/5/012, URL https://doi.org/10.1088%2F0022-3727%2F15%2F5%2F012.

[24] Berger, M., Coursey, J., Zucker, M., Chang, J., Seltzer, S., and Bergstrom, P., "Stopping-Power & Range Tables for Electrons, Protons, and Helium Ions: NIST Standard Reference Database 124," 2017. doi:10.18434/T4NC7P.

[25] Technology, A., "AZ-93 White Thermal Control, Electrically Conductive Paint / Coating," 2004. URL http://www.aztechnology.com/materials-coatings-az-93.html.

[26] Trincavelli, J., and Castellano, G., "The prediction of thick target electron bremsstrahlung spectra in the 0.25–50 keV energy range," *Spectrochimica Acta Part B: Atomic Spectroscopy*, Vol. 63, No. 1, 2008, pp. 1 – 8. doi:https://doi.org/10.1016/j.sab.2007.11.009.

[27] Castellano, G., Osán, J., and Trincavelli, J., "Analytical model for the bremsstrahlung spectrum in the 0.25–20 keV photon energy range," *Spectrochimica Acta Part B: Atomic Spectroscopy*, Vol. 59, No. 3, 2004, pp. 313 – 319. doi:https://doi.org/10.1016/j.sab.2003.11.008, URL http://www.sciencedirect.com/science/article/pii/S0584854703002659.

[28] Sicard-Piet, A., Bourdarie, S., Boscher, D., Friedel, R. H. W., Thomsen, M., Goka, T., Matsumoto, H., and Koshiishi, H., "A new international geostationary electron model: IGE-2006, from 1 keV to 5.2 MeV," *Space Weather*, Vol. 6, No. 7, 2008. doi:10.1029/2007SW000368.

[29] Moore, C. S., Caspi, A., Woods, T. N., Chamberlin, P. C., Dennis, B. R., Jones, A. R., Mason, J. P., Schwartz, R. A., and Tolbert, A. K., "The Instruments and Capabilities of the Miniature X-Ray Solar Spectrometer (MinXSS) CubeSats," *Solar Physics*, Vol. 293, No. 2, 2018. doi:10.1007/s11207-018-1243-3.

[30] "Level 1 Science Data from MinXSS-1 Cubesat," 2017. URL lasp.colorado.edu/home/minxss/data/level-1.

[31] Wentzel, G., "Über strahlungslose Quantensprünge," *Zeitschrift für Physik*, Vol. 43, No. 8, 1927, pp. 524–530. doi: 10.1007/BF01397631, URL https://doi.org/10.1007/BF01397631.

[32] Kahoul, A., Abassi, A., Deghfel, B., and Nekkab, M., "K-shell fluorescence yields for elements with 6<Z<99," *Radiation Physics and Chemistry*, Vol. 80, No. 3, 2011, pp. 369 – 377. doi:https://doi.org/10.1016/j.radphyschem.2010.11.011.

[33] Masterson, R. A., Chodas, M., Bayley, L., Allen, B., Hong, J., Biswas, P., McMenamin, C., Stout, K., Bokhour, E., Bralower, H., Carte, D., Chen, S., Jones, M., Kissel, S., F. Schmidt, M. S., Sondecker, G., Lim, L. F., Lauretta, D. S., Grindlay, J. E., and Binzel, R. P., "Regolith X-Ray Imaging Spectrometer (REXIS) Aboard the OSIRIS-REx Asteroid Sample Return Mission," *Space Science Reviews*, Vol. 214, No. 48, 2018.

[34] Flohrer, T., Krag, H., Klinkrad, H., and Schildknecht, T., "Feasibility of performing space surveillance tasks with a proposed space-based optical architecture," *Advances in Space Research*, Vol. 47, No. 6, 2011, pp. 1029 – 1042. doi: https://doi.org/10.1016/j.asr.2010.11.021.

[35] Scott, R. L., and Ellery, A., "An approach to ground based space surveillance of geostationary on-orbit servicing operations," *Acta Astronautica*, Vol. 112, 2015, pp. 56 – 68. doi:https://doi.org/10.1016/j.actaastro.2015.03.010.

[36] Okajima, T., Soong, Y., Balsamo, E. R., Enoto, T., Olsen, L., Koenecke, R., Lozipone, L., Kearney, J., Fitzsimmons, S., Numata, A., Kenyon, S. J., Arzoumanian, Z., and Gendreau, K., "Performance of NICER flight x-ray concentrator," *Space Telescopes and Instrumentation 2016: Ultraviolet to Gamma Ray*, Vol. 9905, edited by J.-W. A. den Herder, T. Takahashi, and M. Bautz, International Society for Optics and Photonics, SPIE, 2016, pp. 1495 – 1501. doi:10.1117/12.2234436, URL https://doi.org/10.1117/12.2234436.